

# Three dimensional analysis of large strain thaw consolidation in permafrost

Xiaoliang Yao · Jilin Qi · Wei Wu

Received: 24 November 2011 / Accepted: 14 February 2012 / Published online: 23 March 2012  
© Springer-Verlag 2012

**Abstract** Thaw consolidation of ice-rich permafrost is a typical problem in cold regions engineering. This paper proposes a three dimensional analysis of large strain thaw consolidation for post-thawed zone of permafrost, which is defined by a moving thawing boundary problem with phase changes. The theory is implemented in a numerical code and the numerical results are compared with thaw consolidation tests. For problems with low water contents, the small and large strain methods provide virtually the same results. For problems with high water contents, however, the large strain theory shows a much better performance.

**Keywords** Large strain · Numerical simulation · Permafrost · Thaw consolidation

## 1 Introduction

During thaw consolidation of ice-rich frozen soils, a large amount of pore water is drained out of the soil with subsequent decrease in volume, resulting in large settlement. Various investigations on the Qinghai-Tibet highway and railway indicate that continuous thawing of underlying permafrost is one of the main causes of embankment

settlements [5, 16, 25, 26]. The embankment sections damaged by thaw settlement usually lie in sites underlain by permafrost with high ice contents [13]. Thaw settlement is also one of the main causes of structural damage to oil pipelines across permafrost regions [12]. Investigation on the Trans-Alaska pipeline showed that large thaw settlement usually occurred in sections with ice-rich permafrost [24]. Thaw consolidation is a typical large strain problem in cold region engineering. With increasing infrastructures development in permafrost regions, there is urgent need for better understanding of thaw consolidation of frozen soils.

Thaw consolidation of frozen soil is similar to consolidation of unfrozen soil in that both processes are characterized by compression of saturated soil. It is therefore expedient to have a look at the relevant development of consolidation theories for unfrozen soil. One dimensional large strain consolidation theories in convective coordinates were proposed by Mikasa [17] and Gibson et al. [8, 9]. A comparison of these two theories showed that Mikasa's theory can only be applied to the problems with constant loading, while Gibson's theory can be more generally applied to the problem with changing loads [22]. Further experimental and theoretical works have been carried out following Gibson's work [19, 21, 23, 27, 28]. However, most works are limited to 1-D problems.

In order to deal with the large strain consolidation problems with complex boundary conditions, 3-D large strain consolidation theories have been proposed mainly along two lines. Cater et al. [4] formulated a 3-D large strain consolidation theory based on Eulerian description and developed the corresponding finite element code. In this theory, the Cauchy strain rate tensor was used to describe the deformation and Jaumann stress rate was used in the constitutive equation to eliminate the effect of the rigid rotation. Based on Lagrangian description, Chopra [6]

---

X. Yao · J. Qi (✉)

State Key Laboratory of Frozen Soil Engineering, Cold and Arid Regions Environmental and Engineering Research Institute, Chinese Academy of Sciences, 320 Donggang West Road, Lanzhou 730000, China  
e-mail: qijilin@lzb.ac.cn

W. Wu

Institute of Geotechnical Engineering, University of Natural Resources and Life Sciences, Vienna, Feistmantelstrasse 4, 1180 Vienna, Austria

derived the large strain consolidation equations, in which the Piola–Kirchhoff stress tensor and Almansi strain rate were employed to reflect the large strain effects. For consolidation problems involving large strain and strong nonlinearity the Eulerian description seems to provide better results [29].

When dealing with the thaw settlement of permafrost, Foriero and Ladanyi [7] proposed a large strain thaw consolidation theory by combining Gibson’s 1-D large strain consolidation theory with moving boundary defined by a semi-empirical equation according to Nixon and Morgenstern [20]. This paper presents a 3-D analysis of large strain thaw consolidation with complex thawing boundaries dictated by thermal conduction.

### 2 Governing equations and boundary conditions

It is assumed that the thawed regime is saturated. At time  $t_0$  a thawing consolidating soil body occupies the space  $V_0$  with  $S_0$  as its surface (Fig. 1). Part of the surface  $S_{0F}$  is subject to surcharge load, while another part of the surface,  $S_{0P}$  is free for drainage. Suppose that consolidation takes place in the post-thawed domain, while in the frozen domain the displacement and drainage are assumed to be zero. In the area  $S_{0T}$ , the temperature boundary is applied,

while the heat-flux is applied on  $S_{0R}$ . At a later time  $t$ , the body will move to occupy a region in space  $V$  with  $S$  as its new surface. The corresponding boundaries for surcharge load, drainage, temperature and heat-flux are denoted as  $S_F$ ,  $S_P$ ,  $S_T$ , and  $S_R$ , respectively. Throughout the paper we propose that the hydraulic permeability and mechanical properties are independent of temperature. The medium volume expansion related to temperature is not taken into account.

Consider a material point of soil at position  $X_i$  ( $i = 1, 2, 3$ ) at time  $t_0$  in a Cartesian reference frame, at time  $t$  this point will move to a new position  $x_i$  with

$$x_i = X_i + u_i, \quad (i = 1, 2, 3) \tag{1}$$

where  $u_i$  represents the displacement of the material point and is measured relative to the original position in the body at time  $t_0$ .

We proceed to define the kinematic and dynamic variables based on the Eulerian description, i.e. the current configuration is taken as the reference configuration. In the Eulerian description the symmetric deformation rate tensor  $\dot{\epsilon}_{ij}$  and skew-symmetric spin tensor  $\dot{\omega}_{ij}$  are given as,

$$\dot{\epsilon}_{ij} = \left( \frac{\delta v_i}{\delta x_j} + \frac{\delta v_j}{\delta x_i} \right) / 2, \quad \dot{\omega}_{ij} = \left( \frac{\delta v_j}{\delta x_i} - \frac{\delta v_i}{\delta x_j} \right) / 2 \tag{2}$$

where  $v_i$  ( $i = 1, 2, 3$ ) is the instantaneous velocity of the material point. In order to eliminate the effect of rigid rotation, we use the Jaumann stress rate defined by

$$\overset{\vee}{\sigma}_{ij} = \frac{d\sigma_{ij}}{dt} - \sigma_{ik}\dot{\omega}_{ki} - \sigma_{jk}\dot{\omega}_{kj} \tag{3}$$

The constitutive equation can be written as

$$\overset{\vee}{\sigma}_{ij} = D_{ijkl}\dot{\epsilon}_{kl} - \delta_{ij}\dot{p} \tag{4}$$

where  $D_{ijkl}$  is the stress–strain tensor,  $p$  is the pore pressure and  $\delta_{ij}$  is the Kronecker delta. Here, an elastic stress–strain relationship is used to describe the mechanical behavior of soil skeleton, and Eq. 4 can be expressed as

$$\overset{\vee}{\sigma}_{ij} = 2G\dot{\epsilon}_{ij} + (K - 2G/3)\dot{\epsilon}_{ii}\delta_{ij} - \delta_{ij}\dot{p} \tag{5}$$

where  $K$  and  $G$  are the bulk and shear modulus of drained soil.

Assume that the soil skeleton will maintain its structure during consolidation, i.e. transportation and deposition of soil particles are not considered. The Darcy’s law is used to describe the fluid flow through soil,

$$q_i = -k(p/\rho_w g - x_j)_{,j} \tag{6}$$

where  $q_i$  (m/s) is the superficial velocity of the fluid relative to the soil skeleton,  $k$  (m/s) is the hydraulic permeability of soil,  $\rho_w$  (kg/m<sup>3</sup>) is the fluid density and  $g$  (m/s<sup>2</sup>) is the gravity.

It is assumed that the volume change of the soil skeleton is equal to the volumetric difference of the fluid flow into

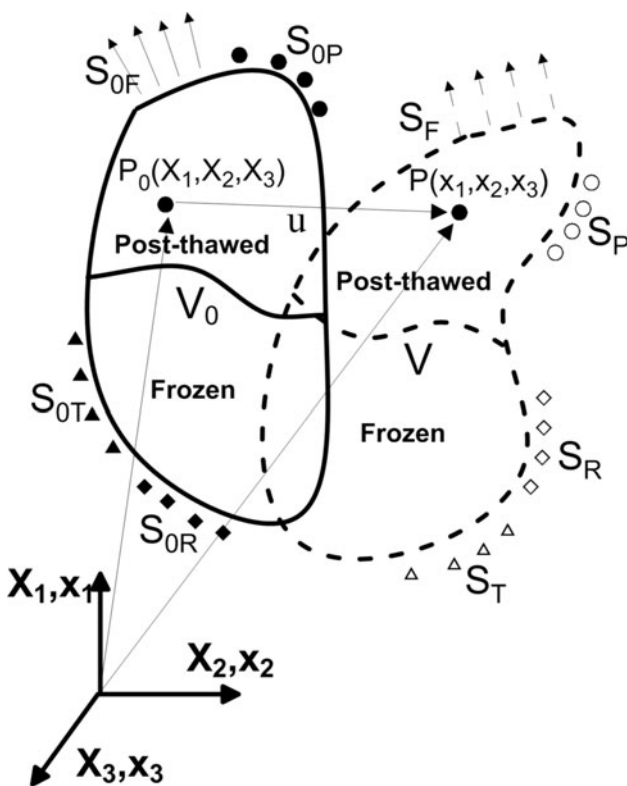


Fig. 1 The thaw consolidation boundary conditions

and out of a material element. Taking into consideration the fluid and solid particle compressibility, the conservation equation can be written as [2]:

$$-q_{vi} + q_v = \frac{1}{M} \frac{\partial p}{\partial t} + \alpha \frac{\partial \varepsilon_v}{\partial t}, \quad \varepsilon_v = \varepsilon_{ii} (i = 1, 2, 3) \quad (7)$$

where  $q_v$  (1/s) is the volumetric fluid source intensity,  $\alpha$  is the Biot’s coefficient,  $M$  (N/m<sup>2</sup>) is the Biot’s modulus. If  $\alpha$  is equal to unity, the grains are considered to be incompressible and the Biot’s modulus  $M$  is equal to  $K_{\omega}/n$ , where  $K_{\omega}$  (N/m<sup>2</sup>) is the fluid bulk modulus and  $n$  is porosity.

The motion of a material element behavior can be described by the balance of its linear momentum,

$$\sigma_{ijj} + \rho g_i = \rho \frac{dv_i}{dt} \quad (8)$$

where  $\rho$  is the medium density.

Equations 1–8 describe the large strain consolidation problem of saturated and compressible media.

All the consolidation calculation must be implemented in the post-thawed domain. It is essential to locate the thaw boundary position. At the earliest, the position of thaw boundary is found from Neumann solution by Carslaw and Jaeger [3], that is

$$X(t) = a\sqrt{t} \quad (9)$$

where  $X$  is the depth to the thaw plane,  $t$  is time, and  $a$  is a constant depending on the thermal properties of soil and temperature boundary conditions [18]. This expression is reasonable for the homogeneous frozen soil subjected to a step increase in temperature at the soil surface. But for the nonhomogeneity and varying surface temperature, Eq. 9 might obtain lower accuracy. Based on this consideration, a more general expression was proposed as [7, 20]

$$X(t) = Ct^n \quad (10)$$

where  $C$  and  $n$  are the constants relating to soil thermal properties and temperature boundary conditions.

However, the semi-empirical expressions for thaw boundary equations 9 and 10 are still only suitable for simple boundary conditions (1-D problem). For complex boundary conditions (3-D problems), the boundary between thawed and frozen domain can be obtained by employing the thermal conductive law considering ice–water phase change of the entire soil body as follows:

$$-h_{vi} + h_v = \rho c \frac{\partial T}{\partial t} (h_i = -\lambda T_f) \quad (11)$$

where the parameters  $c$  and  $\lambda$  are defined by

$$c = \begin{cases} c_u & (T > T_p) \\ c_f + \frac{c_u - c_f}{T_p - T_b} (T - T_b) + \frac{L}{1 + W} \left| \frac{\delta W_i}{\delta T} \right| & (T_b \leq T \leq T_p) \\ c_f & (T \leq T_b) \end{cases} \quad (12)$$

$$\lambda = \begin{cases} \lambda_u & (T > T_p) \\ \lambda_f + \frac{\lambda_u - \lambda_f}{T_p - T_b} (T - T_b) & (T_b \leq T \leq T_p) \\ \lambda_f & (T \leq T_b) \end{cases} \quad (13)$$

where  $h_v$  (W/m<sup>3</sup>) is the volumetric heat source intensity;  $c$  (J/kg °C) is the specific heat considering ice–water phase change,  $c_u$  and  $c_f$  are the specific heat of post-thawed and frozen soil, respectively;  $L$  (J/kg) is the latent heat;  $\lambda$  (W/m °C) is the thermal conductivity,  $\lambda_u$  and  $\lambda_f$  are the thermal conductivity of post-thawed and frozen soil;  $W$  and  $W_i$  (%) are the water and ice content;  $T_p$  and  $T_b$  (°C) are the upper and lower temperature limits of phase change.

For more general expressions of thermal conductivity and specific heat, the readers are referred to Liu and Yu [14].

It is worth mentioning that the freezing temperature for fine soils is often a little lower than 0°C. For simplification, in this paper the 0°C isothermal calculated from Eq. 11 is taken as the thawing boundary.

### 3 Numerical implementation

In Sect. 2, the thaw consolidation governing equations on thermal, fluid and mechanical behaviors are presented. It is convenient to use FLAC3D, which provides the corresponding incremental numerical solutions on those processes, to implement thaw consolidation calculation. However, considering the particularity of thaw consolidation calculation, there are still some challenges to be fulfilled with regard to coupling.

#### 3.1 Temperature dependent thermal properties

In calculation, the specific heat and thermal conductivity are taken as constant by default. According to Eqs. 12 and 13, the two parameters are temperature dependent, as was investigated by Koemle et al. [11]. To make it fulfilled in the embedded programming language, the differential expressions in Eqs. 12 and 13 must be formulated in numerical equations.

According to Xu et al. [30], the ice content in a frozen soil can be written as

$$W_i = W - W_u = W - \theta(T)W_p \quad (14)$$

where  $W_u$  is unfrozen water content,  $\theta(T)$  is a correction coefficient related to soil properties and  $W_p$  is plastic limit water content. For the soil samples (CL) which will be taken as the study object in Sect. 4,  $\theta(T)$  at different temperature can be obtained in Table 1 where correction coefficient up to –10°C is listed so as to show the readers the whole changing tendency, while only the temperature higher than –1°C will be used.

**Table 1** Temperature correction coefficient

Serial number	$T_1$	$T_2$	$T_3$	$T_4$	$T_5$	$T_6$	$T_7$	$T_8$
$T$ (°C)	0	-0.2	-0.5	-1	-2	-3	-5	-10
$\theta$ ( $t$ )	-	0.9	0.65	0.5	0.4	0.35	0.3	0.25

Thus,  $W_i$  at a temperature  $T_m$  ( $m = 2, 3, 4, \dots, 10$ ) can be written as

$$W_{im} = W - \theta(T_m)W_p \tag{15}$$

for  $m = 1$ ,  $W_{i1} = 0$ . According to Table 1, the upper and lower temperature limits ( $T_p$  and  $T_b$ ) of phase change can be valued as 0 and  $-10^\circ\text{C}$ . When  $T_p > T \geq T_b$ , the backward differential form of  $|\frac{\delta W_i}{\delta T}|$  can be written as

$$\left| \frac{\delta W_i}{\delta T} \right|_m = \left| \frac{W_{im} - W_{i(m-1)}}{T_m - T_{(m-1)}} \right| \quad (m = 2, 3, 4, \dots, 10) \tag{16}$$

and  $c$  at  $T_m$  can be written as

$$c_m = c_f + \frac{c_u - c_f}{T_p - T_b}(T_m - T_b) + \frac{L}{1 + W} \left| \frac{\delta W_i}{\delta T} \right|_m \tag{17}$$

as for  $T \geq T_p$  and  $T < T_b$ ,  $c$  is equal to  $c_u$  and  $c_f$ , respectively.

Based on Eqs. 12–17,  $c$  and  $\lambda$  at temperature range  $T_p > T \geq T_b$  can be obtained by linear interpolation as follows

$$\begin{cases} c = \left(1 - \frac{T - T_m}{T_{m+1} - T_m}\right)c_m + \frac{T - T_m}{T_{m+1} - T_m}c_{m+1}, \\ \quad (T_m \leq T \leq T_{m+1}, m = 1, 2, 3, \dots, 10) \\ \lambda = \lambda_f + \frac{\lambda_u - \lambda_f}{T_p - T_b}(T - T_b) \end{cases} \tag{18}$$

After every thermal calculation cycle, Eq. 18 will be activated to reflect the effect of ice-water phase change on thermal conductivity and specific heat.

### 3.2 Fluid and thermal synchronization

In calculation, fluid and thermal calculations are characterized by their own time step ( $\text{fluid}_{dt}$  and  $\text{thermal}_{dt}$ , respectively) and the corresponding times are accumulated separately for the two processes. In thaw consolidation analysis, fluid and thermal process happen in the same time of each calculation cycle. To achieve this goal, one time step must be an integer multiple of the other. In the next section for analysis,  $\text{fluid}_{dt} < \text{thermal}_{dt}$ , the time steps are selected as  $\text{fluid}_{dt} N = \text{thermal}_{dt}$ , where  $N$  is an integer, which means one cycle of coupled analysis includes one thermal step and  $N$  fluid steps. It has been shown that when the calculation step is less than a critical time step, convergence can be guaranteed. Here, the critical time step is

determined by the smallest grid size and thermal and fluid diffusivities [10]. The calculation cycle will stop when the simulation time achieves the target time.

Therefore, a cycle of coupled thermal and consolidation calculation consists of two stages (Fig. 2):

1. Thermal stage: given the initial temperature field at time  $t_0$ , the thermal calculation was performed with a time step and the fluid-mechanical calculation is suppressed.
2. Consolidation stage: the thermal calculation is suppressed and the fluid-mechanical calculation was carried out for  $N$  steps.

### 3.3 Detecting of post-thawed domain

In conventional fluid-thermal-mechanical analysis, the calculation domains for the three processes are usually coincident. However, for thaw consolidation analysis, the thermal and consolidation calculating domains are not compatible. Actually, thermal calculation is implemented in the whole domain, while the consolidation calculation is carried out in the post-thawed domain, which changes continuously throughout the coupled analysis. Therefore, a Fish function must be developed to accomplish this work. In the function, a zone variable (zone\_temp) is used to estimate the thermal status. If  $\text{zone\_temp} \geq 0^\circ\text{C}$ , the zone name is defined as ‘thaw’, and the contrasting is defined as ‘frozen’. The function is activated after every thermal cycle, and the consolidation calculation is implemented in all ‘thaw’ zones. At the same time, in those new ‘thaw’ zones, the corresponding fluid and mechanical properties

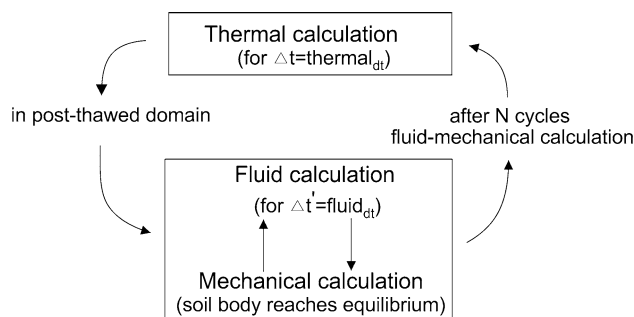


**Fig. 2** The thermal-fluid-mechanical coupling calculation sketch diagram

are assigned and the grid point velocity is set free for allowing deformation.

#### 4 Verification of the theory

The thaw consolidation theory described above is for 3-D problems with complex boundary conditions, which are difficult to simulate by laboratory experiments. For verification and comparison, the thaw consolidation tests were therefore designed and performed under one dimensional conditions. Experiments were carried out to obtain parameters for the calculations on the one hand, and to secure thaw consolidation results on the other hand.

A most frequently encountered silty-clay along the Qinghai-Tibet highway was used as study object, with the liquid and plastic limits of 12.9 and 25.3% (classified as *CL*). Two groups of samples were reconstituted using ice and soil powder mixture, which was then compressed into cylindrical samples in a mold. The samples had a diameter of 10 cm and a height of 10 cm. The dry unit weight and water content of the first sample group were 17.8 kN/m<sup>3</sup> and 19%, respectively, and were considered as samples with low water content in this paper. The second group had a dry unit weight and water content of 10.7 kN/m<sup>3</sup> and 50%, respectively, and were considered as samples with high water content.

Three samples in each group with the same water content were frozen at first. Afterwards, one was for  $K_0$ , i.e. laterally confined compression tests under unfrozen state. The other two were for 1-D thaw consolidation tests. The  $K_0$  tests were carried out on a consolidation apparatus for unfrozen samples. A frozen sample in a plexiglass tube was mounted onto the pedestal of the apparatus with one-side drainage. After the sample is thawed completely, the loads were applied in steps and the corresponding final deformation was recorded. The relationship between loads and strain was obtained. The secant modulus was calculated for each sample according to  $E_s = P_0/\varepsilon_T$ , with  $P_0$  being the surcharge load and  $\varepsilon_T$  the corresponding strain. The dependence of the compression modulus on water content and surcharge load is shown in Fig. 3.

The thaw consolidation tests were carried out on the same apparatus. A frozen sample in the plexiglass tube was directly mounted onto the pedestal of the apparatus with drainage available from the top end. At first, the sample temperature was kept constant at  $-1^\circ\text{C}$  for 4 h. Afterwards, a surcharge load of 50 or 100 kPa was applied. The temperature at the top end of the sample was increased to  $20^\circ\text{C}$  to let the sample thaw, with the bottom end being kept at  $-1^\circ\text{C}$ . Temperature on the plexiglass tube side was

kept at  $0^\circ\text{C}$  which was also the temperature on the side of the soil column, so as to guarantee one dimensionally thawing condition. With the thawing of the sample, the consolidation under load and deformation was recorded. When the displacement change under a certain load is less than 0.01 mm in 1 h, the sample was considered to be stable and the experiment was completed.

#### 4.1 Numerical model

The numerical model was set up according to the test conditions. The temperature and mechanical boundary conditions were kept to be consistent with the corresponding thaw consolidation tests. The model grid dimension was taken as 0.3 cm  $\times$  0.3 cm  $\times$  0.3 cm so as to guarantee the calculation accuracy (Fig. 4). Displacements in X and Y directions were fixed for laterally confined condition. In the Z direction, the displacement was fixed when the nodal temperature is negative; when the nodal temperature became positive, the displacement was set free. Pore water was free to drain only at the top of the model.

The parameters needed for calculation are listed in Table 2. However, the compression modulus  $E_s$  calculated from  $E_s = P_0/\varepsilon_T$  is insufficient for this analysis. For the mechanical analysis in FLAC3D, at least two parameters are needed, i.e. Young modulus ( $E$ ) and Poisson's ratio ( $\nu$ ), by which the bulk and shear modulus in Eq. 5 can be expressed as  $K = E/3(1 - 2\nu)$  and  $G = E/2(1 + \nu)$ , and the Young modulus can be expressed by  $E_s$  as  $E = \beta E_s$ , where  $\beta = 1 - 2\nu^2/(1 - \nu)$ . For the analysis of this 1-D thaw consolidation, the Poisson's ratio has little effect on calculating results, and was taken as 0.3 for the two sample groups. In practical engineering problems, the Poisson's ratio must be measured by testing results.

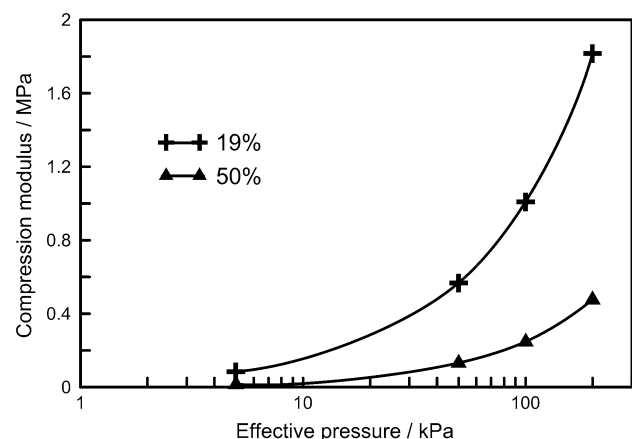
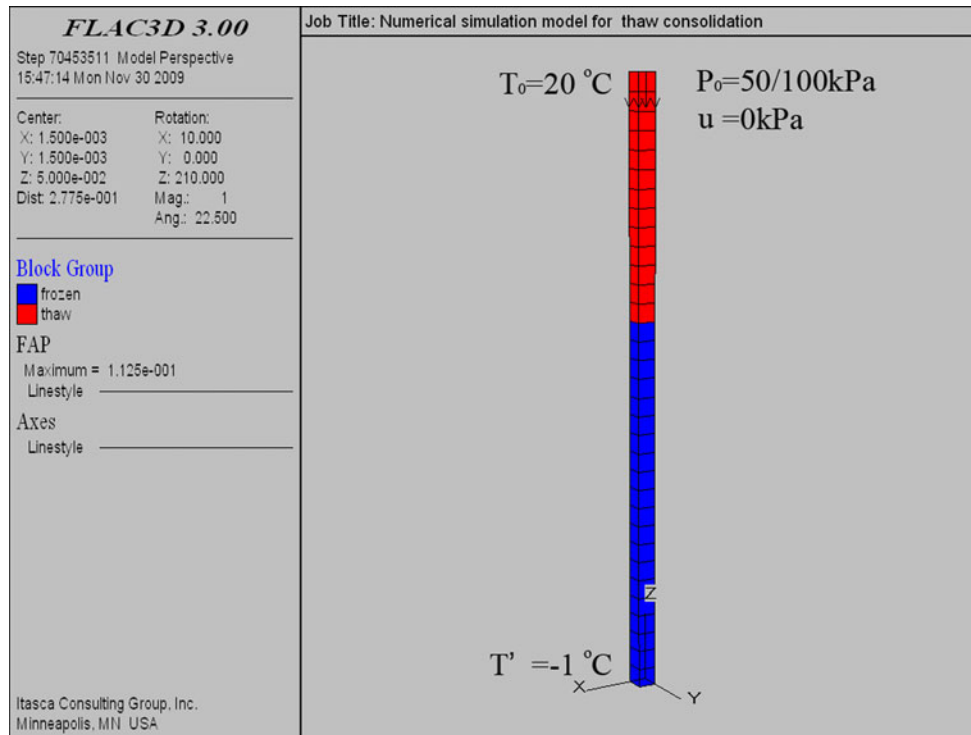


Fig. 3 The compression modulus versus effective pressure



**Fig. 4** The numerical model

As for permeability, it is widely considered to be a function of void ratio  $e$ , i.e.  $k = Ce^D$ , where  $C = \exp(-5.51 - 4\ln(I_p))$ ,  $D = 7.52\exp(-0.25I_L)$ ,  $I_p$  and  $I_L$  are the plastic and liquid indexes [1]. In unfrozen soil, the permeability is usually taken as a constant equal to the average value during consolidating process [8, 9]. But this is not applicable for thaw consolidation analysis.

When frozen soil starts thawing from surface under  $P_0$ , the pore water near the surface will be drained out quickly at first, the consolidation in this area is completed in a very short time and a soil layer with relatively low permeability is formed. Although the newly post-thawed soil has a higher permeability, the drainage rate of the whole thawed soil body depends on the permeability of the boundary layer. Thus, the permeability can be calculated according to  $k = C \cdot e_{p_0}^D$ , where  $e_{p_0}$  is the void ratio when the consolidation under a certain load  $P_0$  is completed.

## 4.2 Comparison of calculation with testing results

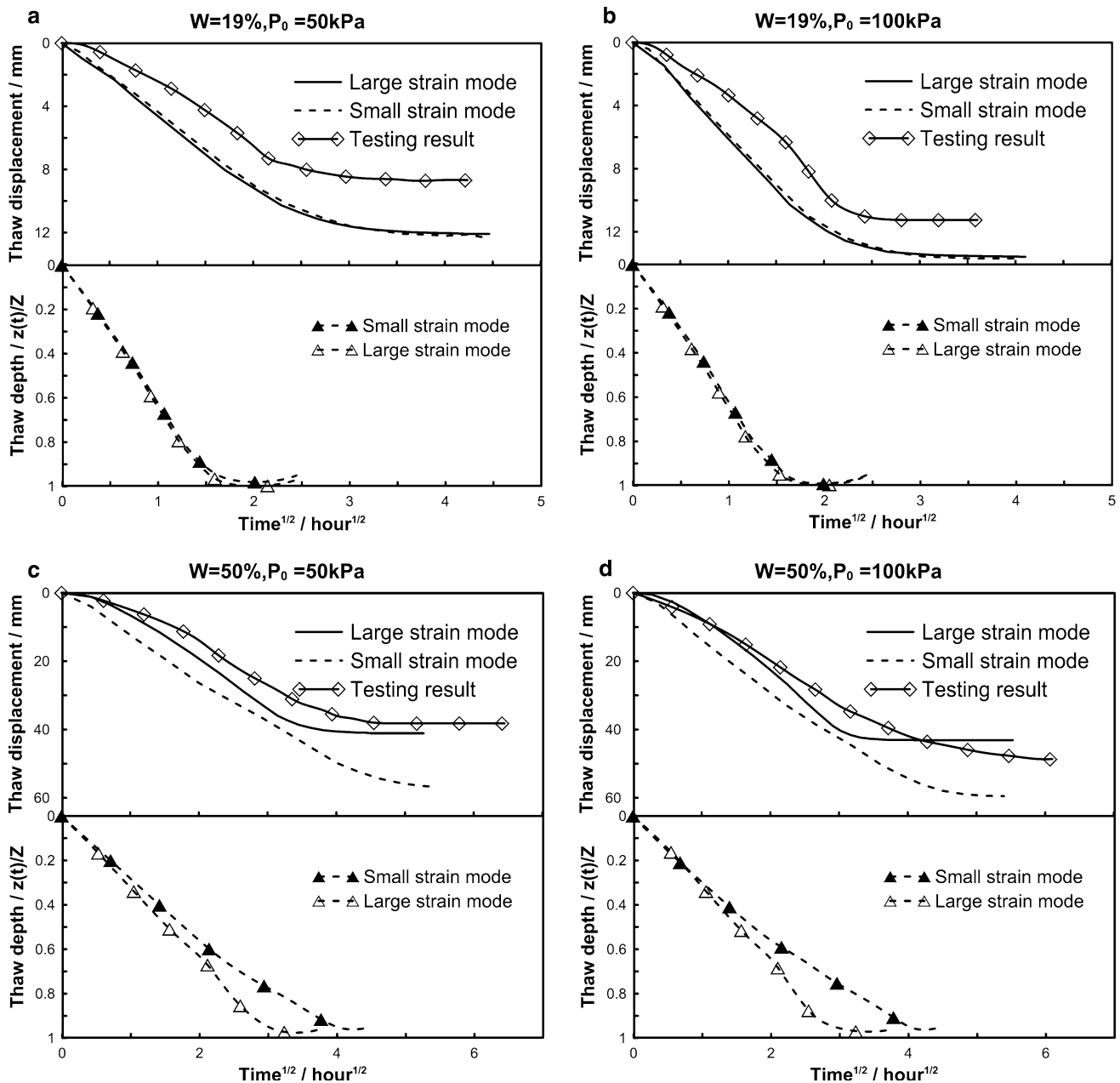
### 4.2.1 Thaw displacement and depth

Figure 5 shows the thaw depth and displacement due to consolidation under 50 and 100 kPa, calculated using both the large and small strain methods. It can be seen in Fig. 5a, b that for the samples with low water content ( $w = 19\%$ ), the large and small strain modes have similar accuracy. For the samples with high water content ( $w = 50\%$ ) in Fig. 5c, d, however, the calculated curves in the small strain and large strain modes show considerable differences. The large strain mode is obviously better than the small strain mode.

According to the previous studies on unfrozen soil, when the volume strain exceeds 10%, the accuracy of small strain theory will decrease considerably [15, 28], because

**Table 2** Parameters used in calculation

Water content (%)	$P_0$ (kPa)	$E_s$ (MPa)	$K$ (m/s)	Poisson's ratio	Specific heat (J/kg °C)		Thermal conductivity (W/m °C)	
					$c_u$	$c_f$	$\lambda_u$	$\lambda_f$
19	50	0.57	7.00e-09	0.3	1,397	1,149	1.24	1.38
	100	1.01	6.02e-09					
50	50	0.13	2.71e-08	0.3	1,953	1,337	1.06	1.98
	100	0.25	1.81e-08					



**Fig. 5** Displacement and thaw depth versus time. Testing results and numerical calculation for samples with two different water contents, and each with two surcharge loads, respectively

the small strain theory based on Cartesian reference frame usually ignores the rigid rotation effect on stress and volume and shape changes. For the 1-D analysis in this paper, rotation is negligible. The reason for the large discrepancy between small strain mode and testing results lies in the fact that the node positions are not updated in the small strain mode.

It is worth pointing out that the thawing depth directly influences the consolidation process, and thus the accuracy of displacement, especially for samples with high water contents. During the thaw consolidation of samples with

low water contents, the heat conductive distance changes slightly when the soil is compressed slightly. Both calculation modes produced similar thawing zones. However, for the samples with high water contents, large strain and compression were obtained, which shortens the heat conductive distance and the rate at which the thawing boundary moves is larger. This could be taken into account in the large strain calculation mode, where the thawing boundary was updated after time steps. Therefore, the thawing rates were distinctly different in the two calculation modes.

#### 4.2.2 Pore pressure

Figure 6 shows the calculated normalized pore pressure distribution at different thaw depth ( $z(t)/Z = 0.3, 0.6$  and  $0.9$ ) with large and small strain modes. Pore pressure at the same normalized initial depth ( $z_{ini}/Z$ ) calculated by both modes are compared. It is interesting that there is only small difference in the pore pressure calculated by the large and small strain modes for all samples. This implies that the changes in volume and shape have little effect on pore pressure distribution. However, the formulation of small and large strain has considerable influence on consolidation process. Figure 7 shows the pore pressure dissipating process at three different depths ( $z_{ini}/Z = 0.3, 0.6$  and  $0.9$ ). Obviously, the pore pressure from large strain calculation dissipates more quickly than that from small strain. This can be explained by the difference in dealing with

volume and shape changes by the two theories. When water content is relatively low, there is only minor change in volume and shape change, and the drainage distance does not change considerably. The change of the dissipation rate of pore pressure remains small. Therefore, even though the small strain mode does not consider the volume and shape changes, the calculated dissipating process still agrees well with that from the large strain mode. However, when the water content becomes larger, the drainage distance shortens considerably as the soil sample is compressed, which influences the dissipating time. This is well reflected by the large strain mode.

To sum up, the thaw depth, displacement and pore pressure are influenced by the changes in volume and shape. The large strain thaw consolidation theory considers the volume and shape changes and has better accuracy than small strain.

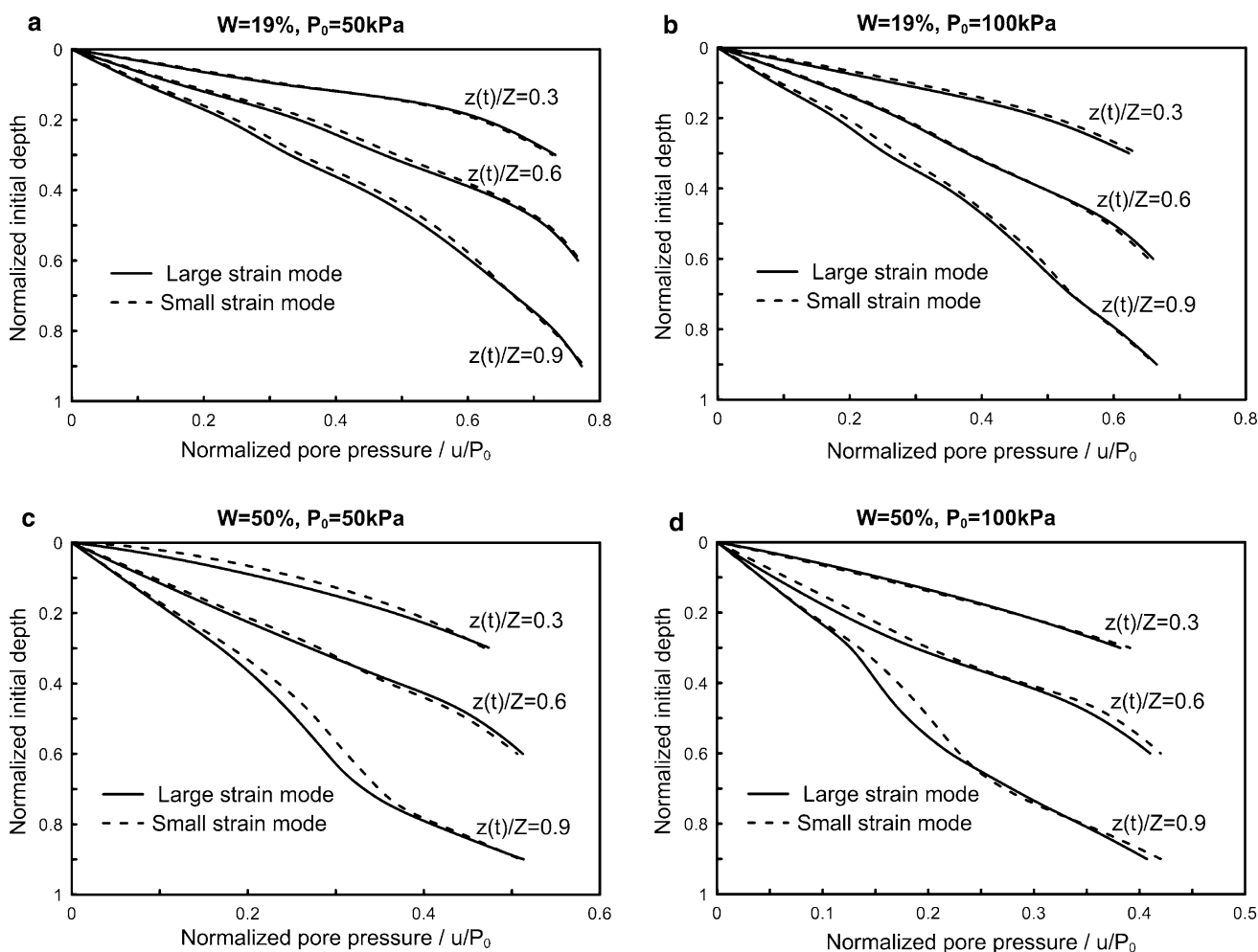


**Fig. 6** Normalized pore pressure versus initial depth. Numerical calculation for samples with two different water contents, and each with two surcharge loads, respectively



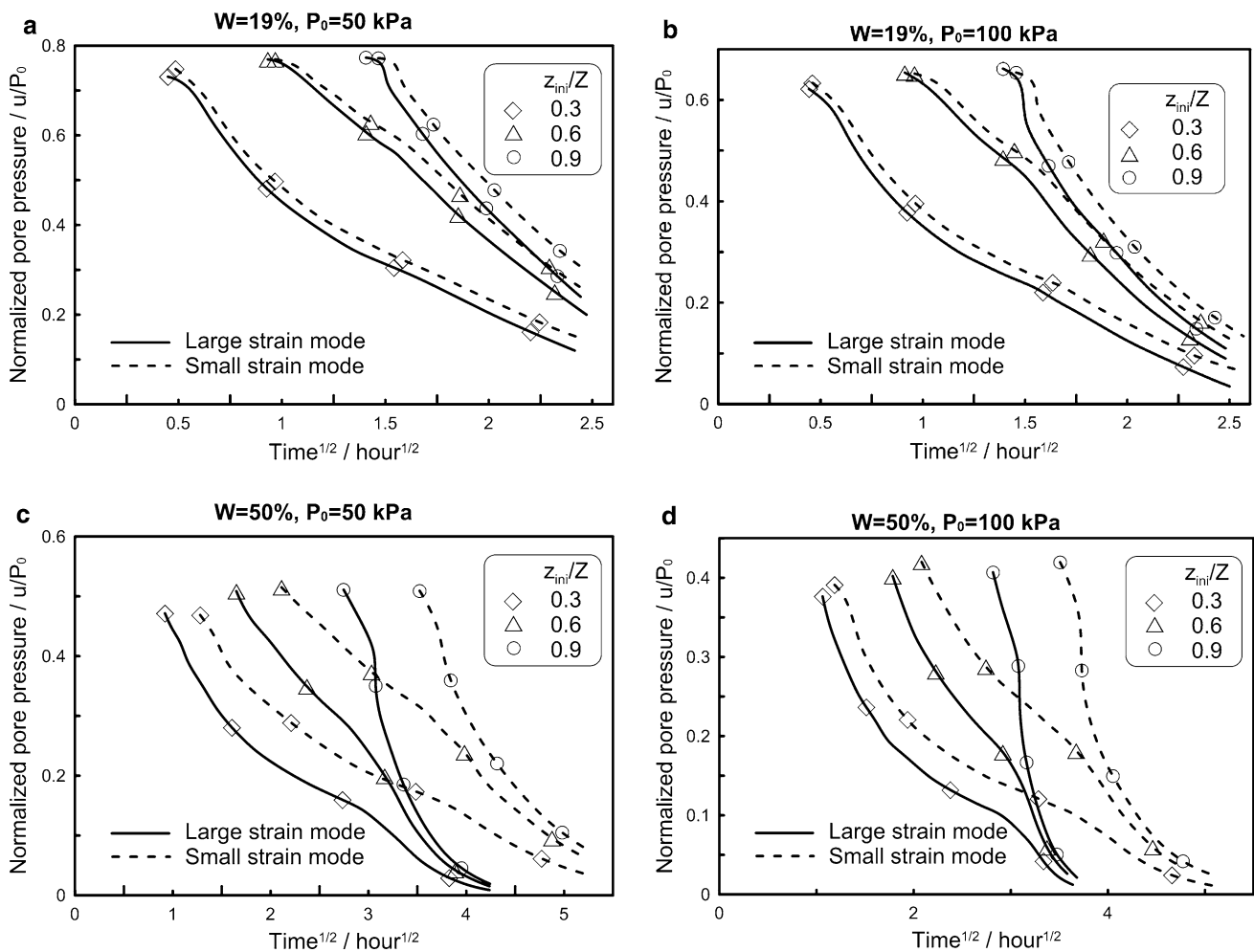


**Fig. 7** Normalized pore pressure versus time. Numerical calculation for samples with two different water contents, and each with two surcharge loads, respectively

## 5 Conclusions

This paper proposes a 3-D large strain thaw consolidation analysis of ice rich frozen soil and the numerical implementation in FLAC3D. Thaw consolidation tests were carried out to verify the theory. Numerical calculations by both small strain and large strain modes were analyzed and compared with the test results.

The large strain theory takes into account the changes in volume and shape during thaw consolidation, the interaction between mechanical, fluid and thermal processes are therefore well simulated. Therefore, the large strain shows better performance in simulating the displacement and pore pressure by taking into consideration of volume and shape changes.

The theory and numerical implementation proposed in this paper provide a useful tool for the prediction of thaw settlement in cold regions engineering especially when the ice-rich permafrost is involved.

**Acknowledgments** This work was supported in part by the 100 Young Talents project of the Chinese Academy of Sciences granted to Dr. Jilin Qi and the National Natural Science Foundation of China (No. 41172253 and 40871039). The authors thank Mr. Geoffrey Gay for his kind help in revising the paper.

## References

- Berilgen SA, Berilgen MM, Ozaydin IK (2006) Compression and permeability relationships in high water content clays. *Appl Clay Sci* 31:249–261
- Biot MA (1973) Non-linear and semi-linear theory of porous solids. *J Geophys Res* 78:4924–4937
- Carslaw HS, Jaeger JC (1947) *Calculation of heat in soils*. Clarendon Press, Oxford
- Carter JP, Small JC, Booker JR (1977) A theory of finite elastic consolidation. *Int J Solids Struct* 13:467–478
- Cheng GD (2005) A roadbed cooling approach for the construction of Qinghai-Tibet Railway. *Cold Reg Sci Technol* 42(2):169–176
- Chopra MB, Dargush GF (1992) Finite element analysis of time-dependent large-deformation problems. *Int J Numer Anal Methods Geomech* 16(2):101–130

7. Foriero A, Ladanyi B (1995) FEM assessment of large-strain thaw consolidation. *J Geotech Eng* 121(2):126–138
8. Gibson RE, England GL, Hussey MJL (1967) The theory of one dimensional consolidation of saturated clays: I. Finite non-linear consolidation of thin homogeneous layers. *Geotechnique* 17(2): 261–273
9. Gibson RE, Schiffman RL, Cargill KW (1981) The theory of one-dimensional consolidation of saturated clays: II. Finite nonlinear consolidation of thick homogeneous layers. *Can Geotech J* 18(2):280–293
10. Itasca (1999) Flac manual: theoretical background. Itasca Consulting Group, Minneapolis
11. Koemle NI, Huetter ES, Feng WJ (2010) Thermal conductivity measurements of coarse-grained gravel materials using a hollow cylindrical sensor. *Acta Geotech* 5:211–223
12. Lachenbruch AH (1970) Some estimates of the thermal effects of a heated pipeline in permafrost. *U.S. Geol Surv Circular* 632:1–23
13. Liu Yongzhi Y, Wu Q, Zhang J, Sheng Yu (2002) Deformation of highway roadbed on permafrost regions of the Qinghai-Tibet plateau. *J Glaciol Geocryol* 24(1):10–15
14. Liu Z, Yu X (2011) Coupled thermo-hydro-mechanical model for porous materials under frost action: theory and implementation. *Acta Geotech* 6:51–65
15. Liu Z, Zhou C (2005) One-dimensional non-linear large deformation consolidation analysis of soft clay foundation by FDM. *Acta Science Arum Naturalium Universitatis Sunyatseni* 4(3):25–41
16. Ma W, Cheng G, Wu Q (2009) Construction on permafrost foundations: lessons learned from the Qinghai–Tibet railroad. *Cold Reg Sci Technol* 59(1):3–11
17. Mikasa M (1965) Consolidation of soft clay. *Jpn Soc Civil Eng*, 21–26
18. Morgenstern NR, Nixon JF (1971) One dimensional consolidation of thawing soils. *Can Geotech J* 8:558–565
19. Morris PH (2003) Compressibility and permeability correlations for fine-grained dredged materials. *J Waterw Port Coast Ocean Eng (ASCE)* 129(4):188–191
20. Nixon JF, Morgenstern NR (1973) Practical extensions to a theory of consolidation for thawing soils. In: *Proceedings of 2nd international Cont. permafrost*. Edmonton, Yakutsk, U.S.S.R., pp 369–377
21. Olson RE (1977) Consolidation under time dependent loading. *J Geotech Eng Div (ASCE)* 103(GT1):55–60
22. Pane V, Schiffman RL (1981) A comparison between two theories of finite strain consolidation. *Soils Found* 21(4):81–84
23. Schiffman RL, Cargill KW (1981) Finite consolidation of sedimenting clay deposits. In: *Proceedings of 10th international conference on Soil Mechanics and Foundational Engineering*, vol 1, pp 239–242
24. Waters E (1974) Heat pipes to stabilize piles on elevated Alaska Pipeline sections. *Pipeline Oil Gas J* 201:46–58
25. Wu QB, Liu YZ, Zhang JM (2002) A review of recent frozen soil engineering in permafrost regions along Qinghai–Tibet Highway, China. *Permafrost Periglacial Process* 13(3):199–205
26. Wu Q, Lu Z, Zhang T, Ma W, Liu Y (2008) Analysis of cooling effect of crushed rock-based embankment of the Qinghai-Xizang Railway. *Cold Reg Sci Technol* 53(3):271–282
27. Xie KH, Leo CJ (2004) Analytical solutions of one-dimensional large strain consolidation of saturated and homogeneous clays. *Comput Geotech* 31:301–314
28. Xinyu Xie, Xiangrong Zhu, Kanghe Xie, Qiuyuan Pan (1997) New Developments of one-dimensional large strain consolidation theories. *Chin J Geotech Eng* 19(4):30–38
29. Xie Y (1998) Large strain consolidation theory and finite element method. China Communications Press, Beijing
30. Xu X, Wang J, Zhang L (2001) Frozen soil physics. Science Press, Beijing